

# Order parameter fluctuations in natural time and $b$ -value variation before large earthquakes

P. A. Varotsos,<sup>1,\*</sup> N. V. Sarlis,<sup>1</sup> and E. S. Skordas<sup>1</sup>

<sup>1</sup>*Solid State Section and Solid Earth Physics Institute,  
Physics Department, University of Athens,  
Panepistimiopolis, Zografos 157 84, Athens, Greece*

## Abstract

Self-similarity may stem from two origins: the process' increments infinite variance and/or process' memory. The  $b$ -value of the Gutenberg-Richter law comes from the first origin. In the frame of natural time analysis of earthquake data, a fall of the  $b$ -value observed before large earthquakes reflects an increase of the order parameter fluctuations upon approaching the critical point (mainshock). The increase of these fluctuations, however, is also influenced from the second origin of self-similarity, i.e., temporal correlations between earthquake magnitudes. This is supported by observations and simulations of an earthquake model.

PACS numbers: 05.40.-a, 89.75.Da, 91.30.Dk, 64.60.av

A large variety of natural systems exhibit irregular and complex behavior which at first look seems to be erratic, but in fact possesses scale-invariant structure, for example see Refs. [1, 2]. A stochastic process  $X(t)$  is called self-similar[3] with index  $H > 0$  if it has the property

$$X(\lambda t) \stackrel{d}{=} \lambda^H X(t) \quad \forall \lambda > 0. \quad (1)$$

where the equality concerns the finite-dimensional distributions of the process  $X(t)$  on the right- and the left-hand side of the equation (*not* the values of the process).

A point of crucial importance in analyzing data from complex systems that exhibit scale-invariant structure, is the following: In several systems this nontrivial structure stems from long-range *temporal* correlations; in other words, the self-similarity originates from the process' memory *only*. This is the case for example of fractional Brownian motion. Alternatively, the self-similarity may solely come from the process' increments *infinite* variance. Such an example is Lévy stable motion (the variance of Lévy stable distributions is infinite since they have heavy tails[4], thus differing greatly from the Gaussian ones). In general, however, the self-similarity may result from both these origins, the presence of which can be in principle identified when analyzing the complex time series in terms of the new time domain termed natural time[5].

The evolution of seismicity is a typical example of complex time series. Several traditional studies found that the  $b$ -value of the Gutenberg-Richter law (see below) decreases before a large event, e.g., see Ref.[6] (cases where  $b$ -value increases prior to and then decreases sharply before a large event have been also reported[7]). Here, considering that the  $b$ -value itself solely focuses on the one origin of self-similarity, and in particular the process' increments infinite variance, we show that, when employing natural time analysis, the  $b$ -value decrease before large earthquakes reflects an increase of the fluctuations of the order parameter of seismicity when approaching the critical point (mainshock, see below). The whole precursory variation of the order parameter fluctuations, however, is more complex since it captures *both* origins. Temporal correlations between earthquake magnitudes *also* play an important role in this precursory variation, thus leading to more spectacular results compared to the ones obtained when restricting ourselves to traditional analysis of  $b$ -value alone.

For a time series comprising  $N$  events we define[8] the natural time  $\chi_k$  for the occurrence of the  $k$ -th event (of energy  $Q_k$ ) by  $\chi_k = k/N$ . We then study the evolution of the pair  $(\chi_k, Q_k)$  where  $p_k = Q_k / \sum_{n=1}^N Q_n$  is the normalized energy released during the  $k$ -th event. In natural time analysis,

the approach of a dynamical system to criticality is identified by means of the variance[5, 8, 9]

$$\kappa_1 \equiv \langle \chi^2 \rangle - \langle \chi \rangle^2 \quad (2)$$

of natural time weighted for  $p_k$  where  $\langle f(\chi) \rangle = \sum_{k=1}^N p_k f(\chi_k)$ . When  $Q_k$  are independent and identically distributed positive random variables, we obtain the “uniform” distribution[10]. In this case, *all*  $p_k$  vary around their mean value  $1/N$  (cf. since  $\sum_{n=1}^N p_n = 1$ ) and the quantity  $\kappa_1$  results in  $\kappa_u = 1/12$  for large  $N$ [10].

In general, in a complex time series, in order to identify the two origins of self-similarity by means of natural time analysis, we focus on the expectation value  $\mathcal{E}(\kappa_1)$  of the variance  $\kappa_1$  of natural time when sliding a natural time window of length  $l$  through a time series of  $Q_k > 0$ ,  $k = 1, 2, \dots, N$ .

If self-similarity exclusively results from the process’ memory, the  $\mathcal{E}(\kappa_1)$  value should *change* to  $\kappa_u = 1/12$  for the (randomly) shuffled data. This is the case of the Seismic Electric Signals (SES) activities[11], which are series of low-frequency ( $\leq 1\text{Hz}$ ) electric signals detected a few to several weeks (up to five months) before an earthquake when the stress in the focal region reaches a *critical* value (and hence long range correlations develop). For example, the upper three channels in Fig.1(b) show three SES activities that preceded major earthquakes in Greece the epicenters of which are depicted in the map of Fig.1(a). On the other hand, if the self-similarity results from process’ increments infinite variance *only*,  $\mathcal{E}(\kappa_1)$  should be the same (but differing from  $\kappa_u$ ) for the original and the (randomly) shuffled data. Finally, when both origins of self-similarity are present, the relative strength of the contribution of the one origin compared to that of the other can be quantified on the basis of Eqs.(12) and (13) of Ref. [12] (see also Ref.[5]).

In what remains we focus on complex time series of seismicity. Earthquakes exhibit scaling relations chief among which is the Gutenberg-Richter (G-R) law [13]. This states that the (cumulative) number of earthquakes with magnitude greater than (or equal to)  $M$ ,  $N(\geq M)$ , occurring in a specified area and time is given by  $N(\geq M) = 10^{a-bM}$ , where  $b$  is a constant, varying only slightly from region to region and the constant  $a$  gives the logarithm of the number of earthquakes with magnitude greater than zero[14]. For reasons of convenience, we write hereafter G-R law into the form  $N(\geq M) \propto 10^{-bM}$ . Considering that the seismic energy  $E$  released during an earthquake is related[15] to the magnitude through  $E \propto 10^{cM}$ , where  $c$  is around 1.5, the latter form turns to the distribution,

$$P(E) \propto E^{-\gamma} \quad (3)$$

where  $\gamma = 1 + b/1.5$ . Hence,  $b \approx 1$  means that the exponent  $\gamma$  is around  $\gamma=1.6$  to  $1.7$ , see Table 2.1 of Ref.[5].

The complex correlations in time, space and magnitude of earthquakes have been extensively studied[16–20]. The observed earthquake scaling laws[21] seem to indicate the existence of phenomena closely associated with the proximity of the system to a *critical* point (e.g., see Ref. [17] and references therein). In the frame of natural time analysis, it has been suggested[9] that the order parameter of seismicity is the quantity  $\kappa_1$ . The  $\kappa_1$  value itself may lead to the determination of the occurrence time of the impending mainshock[5, 8, 12, 22] when SES data are available. In particular, when the  $\kappa_1$  value resulting from the natural time analysis of the seismicity subsequent to the SES recording becomes approximately equal to 0.070, the mainshock occurs within a time window of the order of one week. This procedure was applied for example to the three major earthquakes of Fig.1(a) that followed the SES activities showing in Fig.1(b). In the lack of SES data, we have to solely rely on the fluctuations of the order parameter of seismicity. Along these lines, we investigated[23] the period before and after a significant mainshock. Time-series for various lengths of  $W$  earthquakes that occurred before or after the mainshock have been studied. The probability distribution function (pdf)  $P(\kappa_1)$  versus  $\kappa_1$  was found to exhibit a bimodal feature when approaching a mainshock. To quantify this feature, we considered the *variability* of  $\kappa_1$ , which is just the ratio  $\beta \equiv \sigma(\kappa_1)/\mu(\kappa_1)$  where  $\sigma(\kappa_1)$  and  $\mu(\kappa_1)$  stand for the standard deviation and the mean value for  $\kappa_1$  for sliding window lengths  $l=6-40$ . The bimodal feature reflects that, upon approaching the mainshock (with the number  $W$  of the earthquakes before mainshock decreasing), the variability of  $\kappa_1$  should increase. This was subsequently confirmed since before the M9.0 devastating Tohoku earthquake in Japan on March 11, 2011, the variability of  $\kappa_1$  exhibited[24] a dramatic increase.

In addition, we investigated[25] the order parameter fluctuations, but when considering a natural time window of a fixed-length  $W$  sliding through a seismic catalog (cf. in general the results of complexity measures when considering  $W = \text{const}$  complement[5] those deduced when taking windows of various lengths  $W$ ). For earthquakes in California and Greece, we found[25] that when  $W$  becomes compatible with the lead time of the SES activities (i.e., of the order of a few months), the fluctuations exhibit a global minimum before the strongest mainshock that occurred during a 25- and 10-year period, respectively. A usefulness, among others, of this finding is the following: Once an electric field disturbance has been recorded, but the data are not enough for its secure classification as a SES activity (which demands its recording at a multitude of short- and long-

length measuring dipoles leading to an almost constant electric field value in each direction[11]), the observation of a global minimum in seismicity may be decisive for such a classification. An investigation along these lines of the electric disturbance on January 6, 2012 depicted in the lowest channel of Fig.1(b) is in progress.

Let us now study the interrelation between the  $b$ -value and the variability of  $\kappa_1$ . In particular, we investigate the expected value of  $\kappa_1$  when a natural time window length is sliding through randomly shuffled power law distributed energy bursts that obey Eq.(3). In Fig.2, the pdf  $P(\kappa_1)$  versus  $\kappa_1$  is plotted for several  $b$  values, an inspection of which reveals that: For high  $b$ -values, e.g., for  $b=1.5$  and  $1.4$  the  $P(\kappa_1)$  versus  $\kappa_1$  curve is almost unimodal maximizing at a value somewhat larger than  $0.070$ , while for smaller  $b$  a second mode emerges close to  $\kappa_1 \approx 0$  which reflects that the fluctuations of  $\kappa_1$  are larger. The computed values of the  $\kappa_1$  variability as a function of the  $b$  value are plotted in the inset of Fig.2(b). The general feature of this curve is more or less similar to that observed for example before Tohoku earthquake[24]; quantitative agreement cannot be demanded, however, because *temporal* correlations between the earthquake magnitudes are also present which influence the observed results. This is corroborated by the following results obtained from the Olami-Feder-Christensen (OFC) earthquake model[26].

The OFC model, runs as follows: we assign a continuous random variable  $z_{ij} \in (0, 1)$  to each site of a square lattice, which represents the local ‘energy’. Starting with a random initial configuration taken from a uniform distribution in the segment  $(0,1)$ , the value  $z_{ij}$  of all sites is simultaneously increased at a uniform loading rate until a site  $ij$  reaches the threshold value  $z_{thres}=1$  (i.e., the loading  $\Delta f$  is such that  $(z_{ij})_{max} + \Delta f = 1$ ). This site then topples which means that  $z_{ij}$  is reset to zero and an ‘energy’  $\alpha z_{ij}$  is passed to every nearest neighbor. If this causes a neighbor to exceed the threshold, the neighbor topples also, and the avalanche continues until all  $z_{kl} < 1$ . Then the uniform loading increase resumes. The number of topplings defines the size of an avalanche or “earthquake” and (when it is larger than unity  $k$  increases by one and) is used as  $Q_k$  in natural time analysis. The coupling parameter  $\alpha$  can take values from zero to  $0.25$  and is the *only* parameter of the model, apart from the edge length  $L$  of the square lattice. Here, we use the case of free boundary conditions[27] in which  $\alpha$  varies locally  $\alpha_{ij} = \frac{1}{n_{ij}+K}$ , where  $n_{ij}$  is the actual number of nearest neighbors of the site  $ij$ .

We first study the predictability of the OFC model on the basis of  $\kappa_1$  variability. We consider the variability  $\beta_k$  which is a function of the natural time index  $k$ ,  $k = 1, 2, \dots, N = 2 \times 10^6$  estimated by analyzing in natural time for each  $k$  the preceding  $W = 100$  avalanches. The time increased

probability (TIP)[28] is turned on when  $\beta_k > \beta_c$ , where  $\beta_c$  is a given threshold in the prediction. If the size  $Q_k$  is greater than a target avalanche size threshold  $Q_c$ , we have a successful prediction. For binary predictions, the prediction of events becomes a classification task with two types of errors: missing an event and giving a false alarm. We therefore choose[29] the receiver operating characteristics (ROC) graph[30] to depict the prediction quality. This is a plot of the hit rate versus the false alarm rate, as a function of the total rate of alarms, which here is tuned by the threshold  $\beta_c$ . Only if in between the hit rate exceeds the false alarm rate, the predictor is useful. Random predictions generate equal hit and alarm rate, and hence they lead to the diagonal in ROC plot. Thus, only when the points lie above this diagonal the predictor is useful. As an example, the ROC graphs for  $L = 512$  and  $K = 1$  or  $L = 256$  and  $K = 2$  are shown in Fig. 3. For every given threshold value  $\beta_c$  and a target threshold  $Q_c$ , we get a point in this plot, thus varying  $\beta_c$  we get a curve. The various curves in Fig. 3 correspond to various values of  $Q_c = 168, \dots, 1000$  increasing from the bottom to the top. Since the points in each curve lie above the diagonal, we see that the function  $\beta_k$  exhibits predictive power that *increases* for larger values of  $Q_c$ . In order to investigate the statistical validity of this result, we include in the same graph the results where: (a) the values of  $\beta_k$  were randomly shuffled and the shuffled predictors were used (green curves) and (b) the time-series of  $Q_k$  was randomly shuffled and then  $\beta_k$  was estimated (magenta curves); in both cases, we obtain curves which almost coincide with the diagonal, thus the predictive power of  $\beta_k$  comes from the sequential order of avalanches and it cannot be considered as chancy.

We now proceed to the investigation of the temporal correlations between the magnitudes  $m_k = \log_{10}(Q_k)/1.5$  obtained from the sizes  $Q_k$  of the avalanches in the OFC model preceding a large avalanche. The results can be visualized in two examples in Fig.4 where we plot in blue the exponent  $a_{DFA}$  of the detrended fluctuation analysis (DFA)[31] in natural time (along with the variability  $\beta$  plotted in red) versus the number  $W$  of avalanches before a large avalanche (negative  $x$  semi-axis,  $x = -W$ ). In the upper example, Fig.4(a), the value of  $a_{DFA}$  well before the large avalanche, being somewhat larger than 0.5, exhibits small changes but strongly increases upon approaching the large avalanche, i.e., at  $W = 100$  the value of  $a_{DFA}$  becomes  $\approx 0.75$  which shows intensified *temporal* correlations. In the lower example, Fig.4(b), well before the large avalanche we have  $a_{DFA} \approx 0.6$  showing long range temporal correlations, which first turn to anti-correlations upon approaching the large avalanche, e.g.,  $a_{DFA} \approx 0.43$  at  $W = 400$ , and finally become random, i.e.,  $a_{DFA} \approx 0.5$  at  $W = 100$ , just before the “mainshock”. Hence, we find that both examples of Fig.4, where  $\beta$  rapidly increases upon approaching a large avalanche, show clear precursory

changes in the temporal correlations between avalanches' magnitudes.

---

\* **Correspondence to:** P. Varotsos (pvaro@otenet.gr)

- [1] C. K. Peng, S. V. Buldyrev, A. L. Goldberger, S. Havlin, R. N. Mantegna, M. Simon, and H. E. Stanley, *Physica A* **221**, 180 (1995).
- [2] T. Kalisky, Y. Ashkenazy, and S. Havlin, *Phys. Rev. E* **72**, 011913 (2005).
- [3] J. W. Lamperti, *Trans. Am. Math. Soc.* **104**, 62 (1962).
- [4] A. Weron, K. Burnecki, S. Mercik, and K. Weron, *Phys. Rev. E* **71**, 016113 (2005); N. Scafetta and B. J. West, *Complexity* **10**, 51 (2005).
- [5] P. A. Varotsos, N. V. Sarlis, and E. S. Skordas, *NATURAL TIME ANALYSIS: THE NEW VIEW OF TIME. Precursory Seismic Electric Signals, Earthquakes and other Complex Time-Series* (Springer-Verlag, Berlin Heidelberg, 2011).
- [6] Q. Li, J. Cen, L. Yu, and B. Hao, *Acta Geophys. Sinica* **21**, 101 (1978); M. Imoto, *Tectonophysics* **193**, 311 (1991); Y. Tsukakoshi and K. Shimazaki, *Earth Planets Space* **60**, 915 (2008); K. Katsumata, *Earth Planets Space* **63**, 709 (2011).
- [7] J. Henderson and I. Main, *Geophys. Res. Lett.* **19**, 365 (1992).
- [8] P. A. Varotsos, N. V. Sarlis, and E. S. Skordas, *Practica of Athens Academy* **76**, 294 (2001); *Phys. Rev. E* **66**, 011902 (2002).
- [9] P. A. Varotsos, N. V. Sarlis, H. K. Tanaka, and E. S. Skordas, *Phys. Rev. E* **72**, 041103 (2005).
- [10] P. A. Varotsos, N. V. Sarlis, and E. S. Skordas, *Phys. Rev. E* **67**, 021109 (2003); *ibid* **68**, 031106 (2003).
- [11] P. Varotsos, K. Alexopoulos, and M. Lazaridou, *Tectonophysics* **224**, 1 (1993).
- [12] P. A. Varotsos, N. V. Sarlis, E. S. Skordas, H. K. Tanaka, and M. S. Lazaridou, *Phys. Rev. E* **74**, 021123 (2006).
- [13] B. Gutenberg and C. F. Richter, *Seismicity of the Earth and Associated Phenomena* (Princeton Univ. Press, Princeton, New York, 1954).
- [14] R. Shcherbakov, D. L. Turcotte, and J. B. Rundle, *Geophys. Res. Lett.* **31**, L11613 (2004).
- [15] H. Kanamori, *Nature* **271**, 411 (1978).
- [16] A. Corral, *Phys. Rev. Lett.* **92**, 108501 (2004); J. Davidsen and M. Paczuski, *Phys. Rev. Lett.* **94**, 048501 (2005); A. Saichev and D. Sornette, *Phys. Rev. Lett.* **97**, 078501 (2006).

- [17] J. R. Holliday, J. B. Rundle, D. L. Turcotte, W. Klein, K. F. Tiampo, and A. Donnellan, *Phys. Rev. Lett.* **97**, 238501 (2006).
- [18] J. F. Eichner, J. W. Kantelhardt, A. Bunde, and S. Havlin, *Phys. Rev. E* **75**, 011128 (2007); S. Lennartz, V. N. Livina, A. Bunde, and S. Havlin, *EPL* **81**, 69001 (2008).
- [19] E. Lippiello, L. de Arcangelis, and C. Godano, *Phys. Rev. Lett.* **103**, 038501 (2009); L. Telesca and M. Lovallo, *Geophys. Res. Lett.* **36**, L01308 (2009); N. V. Sarlis, E. S. Skordas, and P. A. Varotsos, *Phys. Rev. E* **80**, 022102 (2009); L. Telesca, *Tectonophysics* **494**, 155 (2010); M. Bottiglieri, L. de Arcangelis, C. Godano, and E. Lippiello, *Phys. Rev. Lett.* **104**, 158501 (2010).
- [20] S. Lennartz, A. Bunde, and D. L. Turcotte, *Geophys. J. Int.* **184**, 1214 (2011); N. V. Sarlis, *Phys. Rev. E* **84**, 022101 (2011).
- [21] D. L. Turcotte, *Fractals and Chaos in Geology and Geophysics* (Cambridge University Press, Cambridge, 1997), 2nd ed.
- [22] P. A. Varotsos et al., *Phys. Rev. E* **73**, 031114 (2006); N. V. Sarlis, E. S. Skordas, M. S. Lazaridou, and P. A. Varotsos, *Proc. Japan Acad., Ser. B* **84**, 331 (2008).
- [23] N. V. Sarlis, E. S. Skordas, and P. A. Varotsos, *EPL* **91**, 59001 (2010).
- [24] P. A. Varotsos, N. V. Sarlis, E. S. Skordas, S. Uyeda, M. Kamogawa, T. Nagao, and H. Tanaka, *Proc. Jpn. Acad., Ser. B* to be published (2012).
- [25] P. A. Varotsos, N. V. Sarlis, and E. S. Skordas, *EPL* **96**, 59002 (2011).
- [26] Z. Olami, H. J. S. Feder, and K. Christensen, *Phys. Rev. Lett.* **68**, 1244 (1992).
- [27] A. Helmstetter, S. Hergarten, and D. Sornette, *Phys. Rev. E* **70**, 046120 (2004).
- [28] V. I. Keilis-Borok and I. M. Rotwain, *Phys. Earth Planet. Inter.* **61**, 57 (1990); V. I. Keilis-Borok and V. G. Kossobokov, *Phys. Earth Planet. Inter.* **61**, 73 (1990).
- [29] A. Garber, S. Hallerberg, and H. Kantz, *Phys. Rev. E* **80**, 026124 (2009).
- [30] T. Fawcett, *Pattern Recogn. Lett.* **27**, 861 (2006).
- [31] C.-K. Peng, S. V. Buldyrev, S. Havlin, M. Simons, H. E. Stanley, and A. L. Goldberger, *Phys. Rev. E* **49**, 1685 (1994).

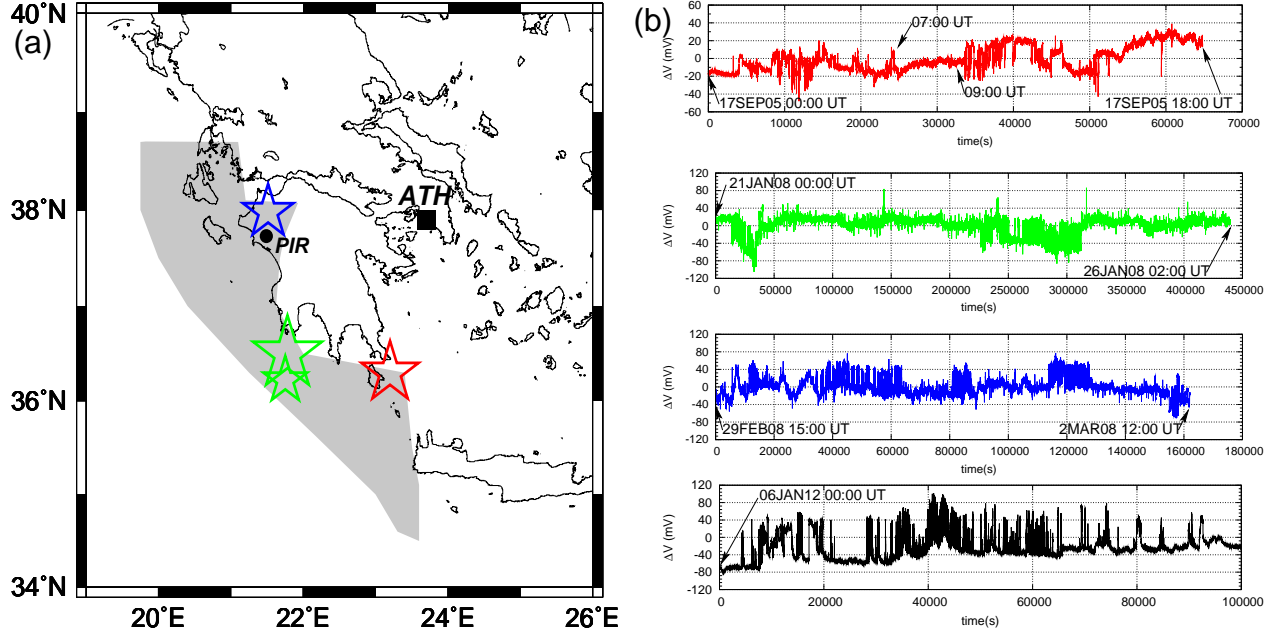


FIG. 1: (color online) (a) Major earthquakes in Greece on January 8, 2006 (red, magnitude  $M_w = 6.7$ ), February 14, 2008 (green,  $M_w = 6.9$  and 6.4) and June 8, 2008 (blue,  $M_w = 6.4$ ) (b) Their preceding SES activities recorded at Pirgos (PIR) measuring station located in western Greece are shown (with the corresponding color) in the upper three channels. The lowest channel depicts a stronger electric disturbance at PIR discussed in the text. Earthquakes with SES activities at PIR are located in the shaded region in (a).

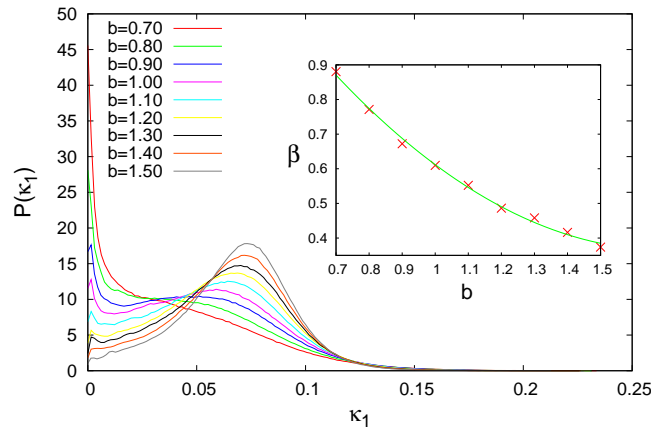


FIG. 2: (color online) The probability density function  $P(\kappa_1)$  versus  $\kappa_1$  for several values of  $b$  for temporally uncorrelated events obeying Eq.(3). The inset depicts the variability  $\beta$  as a function of  $b$ .

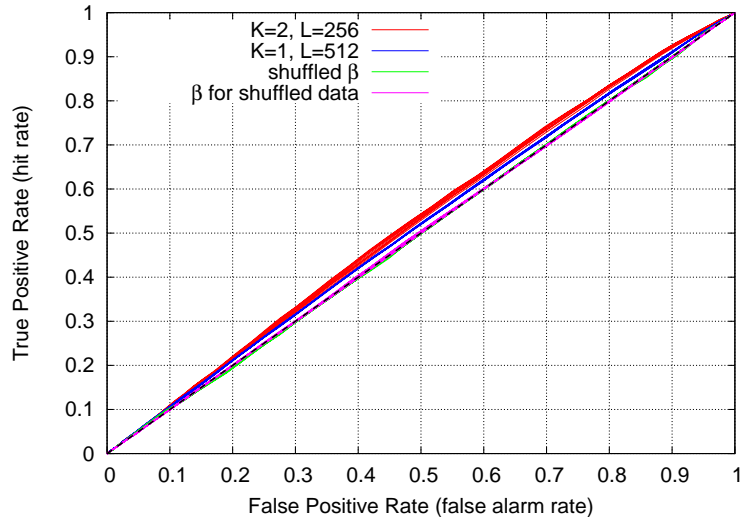


FIG. 3: (color online) The ROC diagram for the OFC earthquake model discussed in the text.

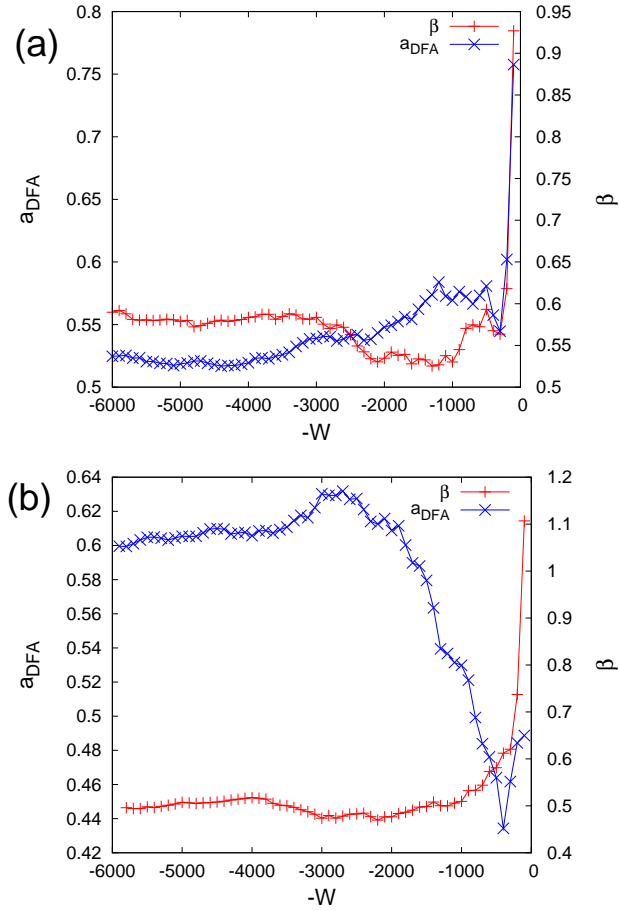


FIG. 4: (color online) The exponent  $a_{DFA}$  (blue, left scale) and the variability  $\beta$  (red, right scale) versus the number of the avalanches preceding a large avalanche,  $Q_k = 40,325$  for (a) and  $Q_k = 31,145$  for (b), that corresponds to  $W = 0$  for the OFC model ( $K = 1, L = 512$ ).